hox gene expression predicts tetrapod-like axial regionalization in the skate, *Leucoraja erinacea*

Katharine E. Criswell[a,b,1], Lucy E. Roberts[a,b], Eve T. Koo[a], Jason J. Head[a,b], and J. Andrew Gillis[a,c]

[a]Department of Zoology, University of Cambridge, Cambridge CB2 3EJ, United Kingdom; [b]University Museum of Zoology, University of Cambridge, Cambridge CB2 3EJ, United Kingdom; and [c]Marine Biological Laboratory, Woods Hole, MA 02543

Edited by Günter Wagner, Department of Ecology and Evolutionary Biology, Yale University, New Haven, CT; received August 6, 2021; accepted November 4, 2021

The axial skeleton of tetrapods is organized into distinct anteroposterior regions of the vertebral column (cervical, trunk, sacral, and caudal), and transitions between these regions are determined by colinear anterior expression boundaries of *Hox5/6*, *-9*, *-10*, and *-11* paralogy group genes within embryonic paraxial mesoderm. Fishes, conversely, exhibit little in the way of discrete axial regionalization, and this has led to scenarios of an origin of *Hox*-mediated axial skeletal complexity with the evolutionary transition to land in tetrapods. Here, combining geometric morphometric analysis of vertebral column morphology with cell lineage tracing of *hox* gene expression boundaries in developing embryos, we recover evidence of at least five distinct regions in the vertebral skeleton of a cartilaginous fish, the little skate (*Leucoraja erinacea*). We find that skate embryos exhibit tetrapod-like anteroposterior nesting of *hox* gene expression in their paraxial mesoderm, and we show that anterior expression boundaries of *hox5/6*, *hox9*, *hox10*, and *hox11* paralogy group genes predict regional transitions in the differentiated skate axial skeleton. Our findings suggest that *hox*-based axial skeletal regionalization did not originate with tetrapods but rather has a much deeper evolutionary history than was previously appreciated.

hox genes | regionalization | chondrichthyan | vertebral column

The axial skeleton (vertebrae and ribs) is a defining feature of the vertebrate body form, and the existence of distinct axial skeletal regions along the anteroposterior (AP) axis of the body is thought to have facilitated evolutionary radiations and ecological specializations across vertebrate phylogeny (1–3). Tetrapod vertebral columns include at least four axial regions: cervical, trunk (further divided into thoracic and lumbar in most mammals and some reptiles), sacral, and caudal, the lengths of which have been modified in different tetrapod groups to suit various ecologies and lifestyles. In mammals and birds, vertebral regions are patterned by *Hox* gene expression within the paraxial mesoderm, and experimental manipulations to anterior *Hox* expression boundaries result in corresponding shifts in vertebral regional boundaries (4–8). For example, in mouse, the anterior expression limit of *Hox10* genes aligns with the thoracic–lumbar transition, and in *Hox10* paralogy group mutants the lumbar vertebrae undergo homeotic transformations to develop ribs, and therefore take on a thoracic identity (5). Additional comparative gene expression studies indicate that this role for *Hox* genes in patterning axial skeletal regions is likely conserved across tetrapods (9–14).

In contrast, the vertebral skeletons of fishes are thought to be less regionalized than those of tetrapods. Historically, the axial skeletons of both bony and cartilaginous fishes were simply subdivided into trunk and tail regions (15–17), but ostariophysan teleosts also possess a Weberian apparatus, a set of specialized anterior vertebrae that transmit sound from the swim bladder to the inner ear (18). Variation in vertebral morphology along the axis, resulting in up to five regions, has also been documented in several actinopterygian species, including chinook salmon (*Oncorhynchus tshawytscha*) (19), ponyfish (*Leiognathus equulus*) (20), and the fossil *Tarrasius problematicus* (21), suggesting that axial regionalization might be more widespread among actinopterygians than previously thought.

hox expression in the paraxial mesoderm has been examined in two teleost fishes with similar vertebral formulae—zebrafish (*Danio rerio*) and stickleback (*Gasterosteus aculeatus*)—and both taxa show nested expression along the AP axis (22, 23). In zebrafish, *hox* expression is initially dynamic but stabilizes at the 20-somite stage (22, 24). In both zebrafish and stickleback, the anterior limit of *hoxc6* expression appears to mark the transition to the first rib-bearing vertebra, and in zebrafish the transition from rib-bearing to hemal arch-bearing (i.e., trunk to tail) vertebrae correlates with the anterior expression of *hoxa12* (22, 25). Anterior expression limits of other *hox* genes from paralogy groups 7 to 11 all align with somites that contribute to the rib-bearing trunk region, however, and have no discrete anatomical correlates (22, 25–27). *hox13* paralogs are expressed in the tail bud in zebrafish (28) and mutation of *Hoxb13* results in the addition of two caudal vertebrae in mice (29), but there is no evidence relating *hox13* expression to morphological changes in the caudal fin vertebrae of teleosts. These studies indicate that, despite evidence of some degree of axial regionalization in actinopterygians, teleost *hox* gene expression patterns are complex and difficult to relate to changes in vertebral morphology. Within cartilaginous fishes, nested AP *hox* expression has been demonstrated in the catshark (*Scyliorhinus canicula*) (30, 31). Moreover, regionalization of the axial skeleton of the thorny skate (*Amblyraja radiata*) was reported based on discrete

Significance

The tetrapod vertebral skeleton is subdivided into distinct regions that are determined by spatial expression of *Hox* genes in the early embryo. Fishes are thought to lack comparable regionalization, but the relationship between anatomy and *hox* expression has not been tested beyond tetrapods. By comparing vertebral morphology with embryonic *hox* expression in a cartilaginous fish, the skate (*Leucoraja erinacea*), we found that the skate vertebral column is regionalized, with regional transitions predicted by embryonic *hox* gene expression patterns. This discovery points to an origin of nested *hox* gene expression and *hox*-based vertebral regionalization at the common ancestor of jawed vertebrates.

Author contributions: K.E.C., J.J.H., and J.A.G. designed research; K.E.C. and E.T.K. performed research; L.E.R. contributed new analytic tools; K.E.C. and L.E.R. analyzed data; and K.E.C., J.J.H., and J.A.G. wrote the paper.

The authors declare no competing interest.

This article is a PNAS Direct Submission.

[1]To whom correspondence may be addressed. Email: kc518@cam.ac.uk.

This article contains supporting information online at http://www.pnas.org/lookup/suppl/doi:10.1073/pnas.2114563118/-/DCSupplemental.

Published December 13, 2021.

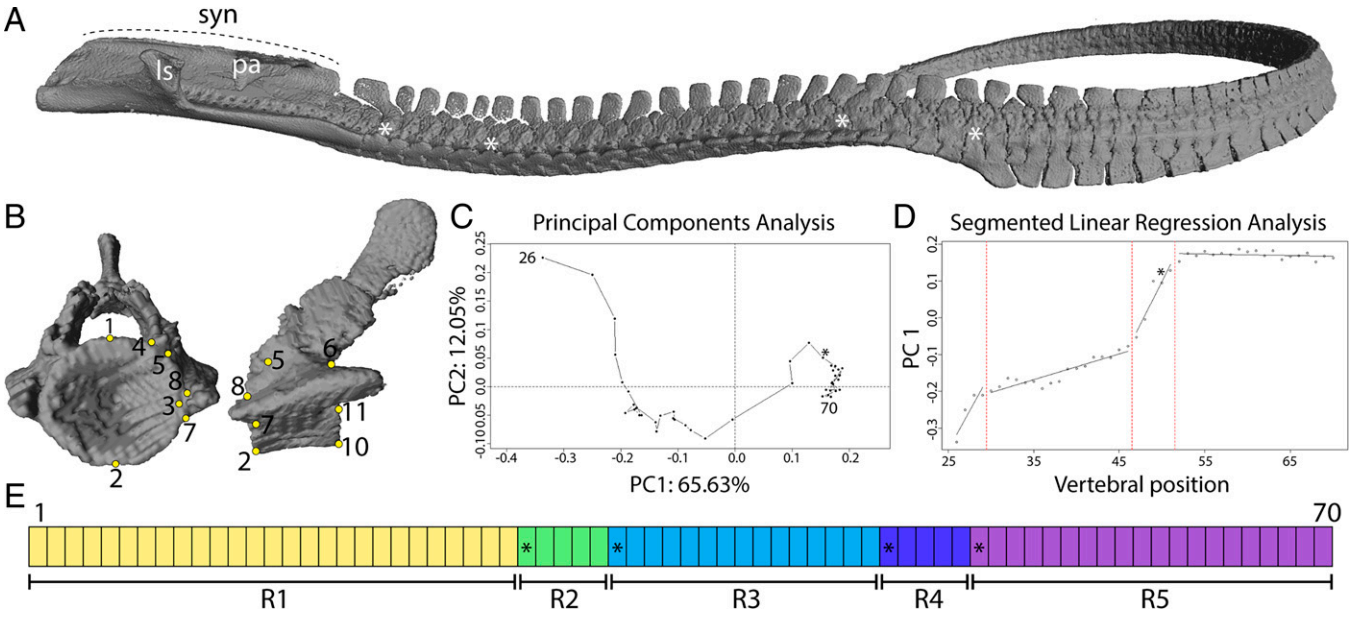

Fig. 1. Regionalized vertebral skeleton of the little skate. (*A*) Three-dimensional rendering of a microCT scan showing the entire vertebral column of an adult skate. (*B*) Skate trunk vertebra showing landmarks used for geometric morphometrics. (*C*) Example plot from PC analysis for skate vertebrae showing vertebrae 26 to 70. (*D*) Segmented linear regression plot showing postsynarcual region breaks at vertebrae 29, 46, and 51. (*E*) Region model showing synarcual vertebrae (R1), anterior transitional region (R2), trunk region (R3), posterior transitional region (R4), and tail region (R5). Asterisks mark the first vertebra in each region from R2 onward, in *A* and *E*, and the trunk-to-tail transition in *D*. ls, lateral stay articulation; pa, pectoral arch; syn, synarcual.

morphological characteristics of vertebrae along the AP axis (32). However, evidence linking *hox* expression boundaries to changes in vertebral morphology along the axis in cartilaginous fishes is lacking. It therefore remains unclear what role *Hox* genes might have played in the evolution of vertebral complexity.

To test whether the tetrapod *Hox* code—and its role in establishing axial regions within the vertebral skeleton—has a deeper evolutionary origin within vertebrates, we investigated *hox* gene expression and axial skeletal regionalization in a cartilaginous fish, the little skate (*Leucoraja erinacea*). As a sister taxon to bony vertebrates, comparative studies of skate development facilitate inference of anatomical and developmental conditions in the last common ancestor of jawed vertebrates, and our previous work on skate axial skeletal development allows us to confidently relate somite to vertebral identity along the AP axis (33–35). Contrary to previous assumptions of relative axial skeletal homogeneity, our quantitative assessment of morphology reveals that the skate vertebral column possesses at least five distinct axial regions, with regional boundaries predicted by tetrapod-like patterns of *hox* gene expression within embryonic somitic mesoderm. This suggests that core elements of the mechanism governing tetrapod axial skeletal regionalization have been conserved for ∼500 million y from the origin of jawed vertebrates.

Results

Morphometric Analysis Reveals Five Axial Skeletal Regions in Skate. We first determined the extent of skate axial skeletal regionalization. The little skate vertebral column includes a synarcual, which is composed of ∼25 fused anterior vertebrae (determined by counts of spinal nerve foramina) that support the pectoral girdle and pectoral fin-based locomotion in skates (Fig. 1*A*) (36). Projecting laterally from the ventral midpoint of the synarcual are two articulations for the lateral stays, rectangular cartilages that stabilize the pectoral girdle. The pectoral arch extends laterally just posterior and dorsal to these processes to fuse to the scapulocoracoid of the pectoral girdle (37). The fused nature of the synarcual prevented us from placing landmark coordinates on each individual vertebra, and so our analysis of regionalization therefore began at the first vertebra posterior to the synarcual, vertebra 26. To test for regionalization, we performed Procrustes superimposition of microcomputed tomography (microCT)–rendered morphology for vertebrae caudal to the synarcual, up to vertebra 70 in three adult skates. We quantified vertebral morphology as homologous landmarks represented by three-dimensional (3D) Cartesian grid coordinates (Fig. 1*B* and *SI Appendix*, Table S1) and used principal-component (PC) scores of realigned landmark coordinates as shape variables. To test for region numbers and boundaries, we performed segmented linear regression on PC scores and used maximum-likelihood model selection to determine the best fit number of regions within the quantified axial skeleton, where individual regression slopes indicate regions and slope breaks represent region boundaries (*SI Appendix*, Fig. S1 and Table S2) (3, 38). PC analysis revealed a shape gradient along the AP axis of the vertebral column in the skate (Fig. 1*C* and *SI Appendix*, Fig. S1 *A*–*C*), with a four-region model having the best fit to the gradient, and an overall best model of five regions with boundaries at approximately vertebrae 26, 31, 46, and 51 when we included the synarcual as the first region (Fig. 1 *D* and *E* and *SI Appendix*, Fig. S1 *A′*–*C′* and *D* and Table S2). To account for changes in shape not attributable to size-scaling developmental processes such as intracolumnar variation in growth rates, we conducted regionalization analyses using residuals from regression of PC scores against centroid size for each vertebra. We recovered nearly identical results, with average region boundaries within one vertebra of the original analysis (*SI Appendix*, Fig. S1 *A″*–*C″* and *E*). Skates therefore appear to possess at least five distinct axial regions, hereafter referred to as R1 to R5: the synarcual; a short transitional region of approximately five vertebrae between the synarcual and the trunk; a trunk region of ∼15 vertebrae; a short transitional region of approximately five vertebrae between the trunk and the tail; and a tail region extending to vertebra 70 (the posterior-most element in our analysis).

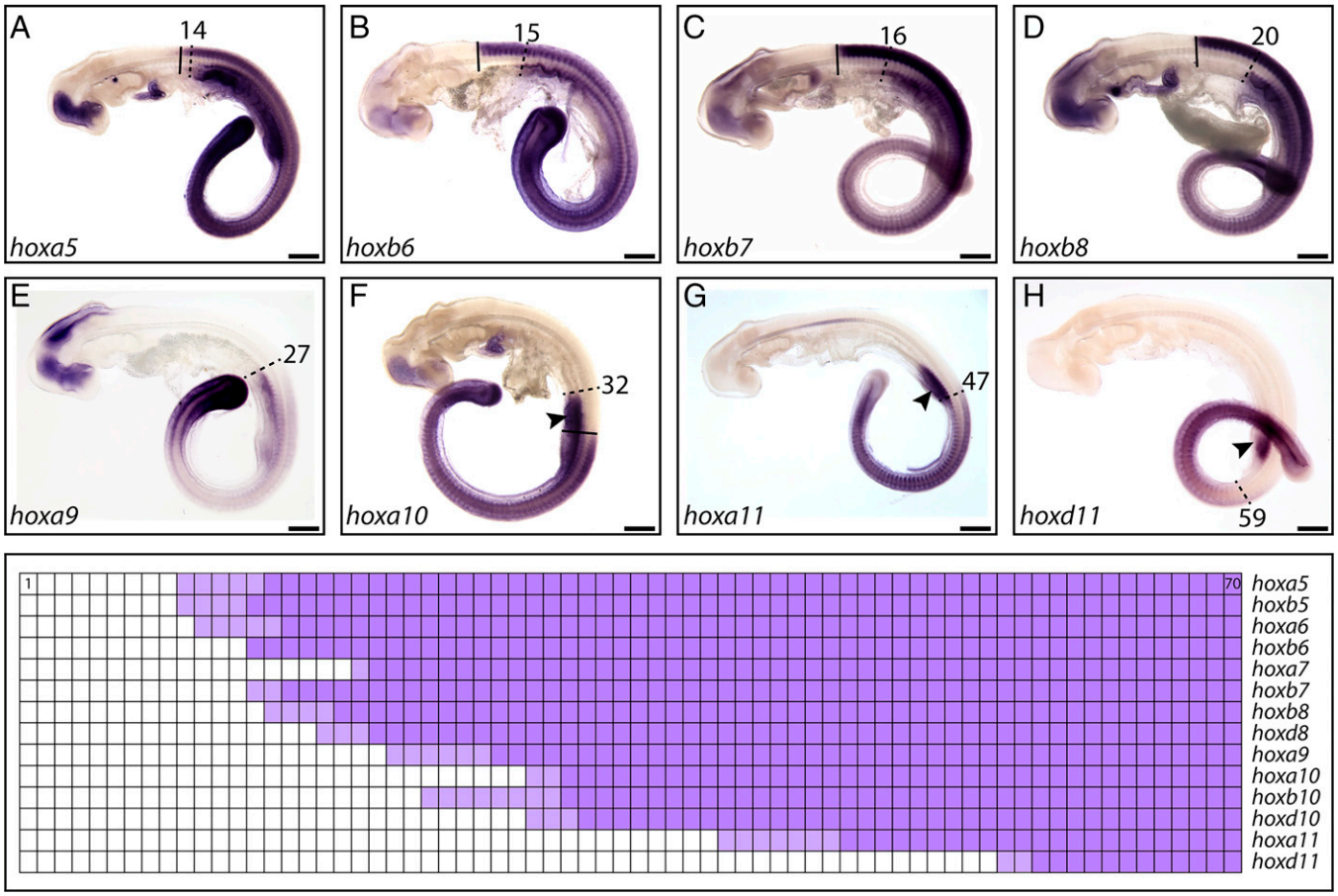

Fig. 2. Nested expression of *hox* genes during somitogenesis in the little skate. Representative examples of whole-mount mRNA ISH experiments at Stage 18. (*A*) *hoxa5* has an anterior expression boundary at somites 14 and 15. (*B*) *hoxb6* is expressed up to somites 13 and 14. (*C*) *hoxb7* with expression boundary at somites 14 to 16. (*D*) *hoxb8* with anterior expression up to somites 19 to 21. (*E*) *hoxa9* with anterior expression up to somites 27 to 29. (*F*) *hoxa10* with anterior expression up to somites 31 to 33. (*G*) *hoxa11* with anterior expression up to somite 50. (*H*) *hoxd11* with anterior expression up to somites 58 to 60. (*Bottom*) Lighter boxes indicate somites with variable expression such as a temporal shift or variation between individuals (see *SI Appendix*, Table S4 for details). Dashed lines indicate the anterior-most extent of expression in the somites, while solid lines indicate the anterior extent of expression in the neural tube, where this differs from the anterior boundary of somite expression. Arrowheads indicate expression in the incipient cloaca. (Scale bars, 500 μm.)

Nested Expression of *hox* Genes in Skate Somitic Mesoderm. We next tested for nested expression of *hox* genes during somitogenesis in skate embryos. Skates possess 34 *hox* genes, organized into three clusters (*hoxa*, *b*, and *d*) (39). We performed chromogenic whole-mount messenger RNA (mRNA) in situ hybridization (ISH) experiments for selected *hox* genes from paralogy groups 5 to 11 in embryonic stage 18 (S18), S20, S22, and S25. These stages were selected as they span the onset to termination of somitogenesis (Fig. 2 and *SI Appendix*, Fig. S2 and Table S3). Anterior expression boundaries for each *hox* ortholog were then determined by somite counts, assisted by DAPI staining (using both bright-field and fluorescence microscopy).

Expression boundaries for *hoxa5*, *hoxb5*, *hoxa6*, and *hoxb6* were similar from S18 to S22, with the anterior expression limits ranging from somite 13 to 16 (*SI Appendix*, Fig. S2 *A–D* and Table S3). By S25, anterior expression limits of *hoxa5* and *hoxb5* extend slightly anteriorly relative to *hoxa6* and *hoxb6*, to the level of somite 10 (*SI Appendix*, Fig. S2 *A–D* and Table S3). *hoxa7* was expressed consistently up to somites 21 and 22 in all stages examined (*SI Appendix*, Fig. S2*E* and Table S3), while the anterior limit of *hoxb7* expression aligned with somites 14 to 16 (*SI Appendix*, Fig. S2*F* and Table S3). *hoxb8* and *hoxd8* were both expressed up to somites 19 to 22 for all stages examined (*SI Appendix*, Fig. S2 *G* and *H* and Table S3), while the anterior limit of *hoxa9* expression aligned with somites 24 to 29 (*SI Appendix*, Fig. S2*I* and Table S3). *hoxb10* was expressed up to the level of approximately somite 25 in S18 (*SI Appendix*, Fig. S2*K* and Table S3), with this anterior expression boundary shifting caudally to somites 31 to 34 from S20 to S25, while *hoxa10* and *hoxd10* were expressed consistently to the level of somites 31 to 34 in all stages (*SI Appendix*, Fig. S2 *J* and *L* and Table S3). Finally, *hoxa11* was expressed up to approximately somites 46 to 49 in S20 and S22 (which corresponds to the posterior margin of the cloaca), shifting to somites 42 to 47 in S25 (*SI Appendix*, Figs. S2*M* and S3 and Table S3), while *hoxd11* was expressed up to somites 58 to 60 in all stages (*SI Appendix*, Fig. S2*N* and Table S3). Overall, these experiments reveal patterns of *hox* gene spatial nesting in skate somitic mesoderm that are more similar to the broadly spaced and nested AP expression of tetrapods (4, 11–13) than to the compacted expression boundaries seen in teleosts (22, 23, 26, 27).

***hox* Expression Boundaries Correlate with Regional Transitions in the Skate Vertebral Column.** We tested whether the anterior *hox* expression boundaries noted above correspond to morphometric regional transitions in the differentiated vertebral skeleton. In the skate, relationships between somites and vertebrae have been established in the trunk and tail (35). However, the

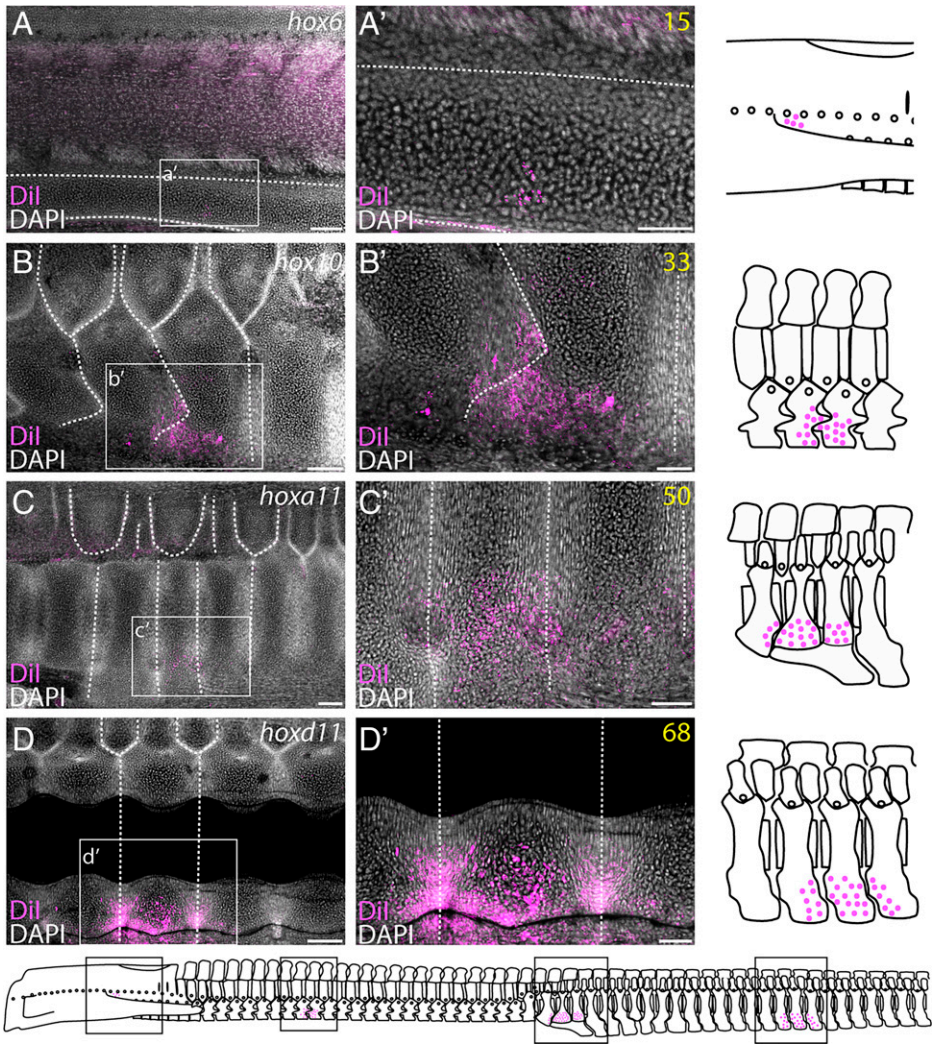

Fig. 3. Fate mapping of anterior *hox* expression boundaries in the little skate. Sagittal sections of S32 skate embryo vertebrae showing results of *hox* gene boundary fate-mapping experiments. (*A* and *A′*) Experiment marking *hox6* expression boundary (~somite 15) showing CM-DiI recovered in the fused cartilage of the synarcual. (*B* and *B′*) Experiment marking *hox10* expression boundary (~somite 32) showing CM-DiI in two successive trunk vertebrae. (*C* and *C′*) Experiment marking *hoxa11* expression boundary (~somite 50) showing CM-DiI in the first three postcloacal vertebrae, marking the transition from the trunk to the tail. (*D* and *D′*) Experiment marking *hoxd11* expression boundary (~somite 59) showing CM-DiI recovered in three tail vertebrae. (*Right*) Line drawings showing the vertebral morphology and approximate location of CM-DiI in each experiment. (Scale bars, 100 μm [*A–D*] and 50 μm [*A′–D′*].)

number of somites contributing to the chondrocranium is not known, and this hinders direct comparisons between somite number and eventual vertebral position. To more precisely test for relationships between anterior *hox* gene expression boundaries and axial skeletal regional transitions in skate, we conducted a series of somite fate-mapping experiments to serve as reference points between somites and the differentiated axial skeleton. Somites were labeled with the lipophilic dye CM-DiI at four positions along the AP axis: somites 13 to 15, 31 to 33, 48 to 50, and 58 to 60 (roughly corresponding to the anterior expression boundaries of *hoxa6*/*hoxb6*, *hoxa10*/*hoxb10*/*hoxd10*, *hoxa11*, and *hoxd11*). These positions were selected to test for potentially shared correspondence of *hox* expression boundaries and anatomical transitions between tetrapods and skate, and to span the AP axis of the skate embryo (thereby allowing us to confidently infer anatomical correlates of expression boundaries sitting rostral or caudal to our reference points). We then reared injected embryos to the point of axial skeletal differentiation and recovered and mapped labeled derivatives of our initial somite injections within the axial column (*SI Appendix*, Fig. S4).

We found that in the trunk, injection of a particular somite, counting from the first somite, led to labeling of nearly the same numbered vertebra, counting from the first vertebra posterior to the chondrocranium. This close correspondence suggests that, in contrast to tetrapods, there is limited somitic contribution to the chondrocranium, and that somite number therefore aligns closely with vertebral number [albeit with the half-somite shift resulting from resegmentation (35)]. Our CM-DiI injection at the level of somites 13 to 15 (corresponding to the anterior boundary of *hox* paralogy group 5 and 6 expression) resulted in the recovery of CM-DiI-labeled chondrocytes in the middle of the synarcual, corresponding to the posterior margin of the lateral stay and anterior margin of the pectoral arch (Fig. 3 *A* and *A′*). Next, our CM-DiI injection at the level of somites 31 to 33 (corresponding to the anterior boundary of *hox* paralogy group 10 expression) gave rise to CM-DiI-labeled chondrocytes in vertebrae 32 to 35 (i.e., at the R2–R3 boundary; Fig. 3 *B* and *B′*). Furthermore, by counting somites rostrally from this injection site, we were able to infer from this experiment that the anterior limit of *hoxa9* expression (approximately somites 24 to 29) corresponds to the posterior margin of

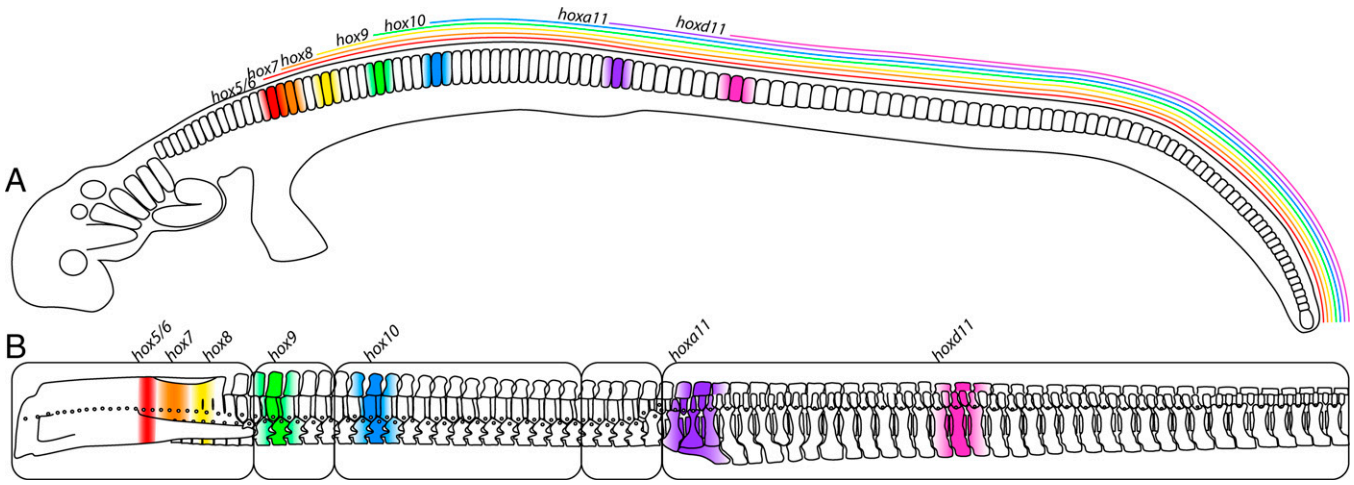

Fig. 4. *hox* expression boundaries predict vertebral regional boundaries in the little skate. Schematic showing (*A*) anterior expression boundaries of *hox* gene paralogy groups 5 to 11 in an S25 skate embryo (at the end of somitogenesis) and (*B*) the location of corresponding vertebrae in the differentiated vertebral column of a hatchling little skate. Regions are marked by rounded boxes.

the synarcual (i.e., the R1–R2 boundary). Our CM-DiI injection at the level of somites 48 to 50 (corresponding to the posterior portion of the cloaca and the anterior limit of *hoxa11* expression) gave rise to CM-DiI-labeled chondrocytes at the level of vertebrae 49 to 51 (i.e., at the R4–R5, or trunk–tail, boundary; Fig. 3 *C* and *C′*). Finally, CM-DiI injection at the level of somites 58 to 60 (corresponding to the anterior boundary of *hoxd11* expression) resulted in CM-DiI-labeled chondrocytes within vertebrae 62 to 68 (Fig. 3 *D* and *D′*). The latter were located within the diplospondylous tail region, where each somite contributes to three vertebrae (35), and did not correspond to an axial skeletal regional transition. Taken together, our fate-mapping results show that three of the four region boundaries identified in our segmented linear regression analysis are predicted by anterior limits of *hox* gene or paralogy group expression within the somitic mesoderm— with an additional *hox* expression boundary corresponding to the projecting articulation for the lateral stays and pectoral arch within the synarcual (Fig. 4).

Discussion

The regionalization of the skate vertebral column that we report here stands in stark contrast to the conventional view of a simple distinction between trunk and tail vertebrae in fishes. Rather, our findings, along with reports of striking axial skeletal complexity and regionalization in some extinct and extant fishes (19–21, 32), point instead to greater ancestral axial skeletal complexity than is currently recognized for jawed vertebrates. While the tail region of the skate axial column is easily recognizable by the change in morphology from laterally projecting transverse processes to ventrally directed hemal arches, the more rostral vertebral regions vary more subtly in morphology. The morphometric approaches used here have recently resolved cryptic anatomical boundaries in the vertebral skeletons of tetrapod taxa previously thought to have lost axial regionalization (38), and have allowed for finer-scale resolution of regional boundaries in fossil lineages (3). If applied more widely, comparative morphometric approaches can help to detect cryptic regionalization in a much broader array of taxa, providing a more comprehensive picture of the evolutionary history of axial regionalization.

Skates also exhibit nesting of paraxial mesodermal *hox* gene expression consistent with characterization of *hox* expression in the dogfish shark, *Scyliorhinus canicula* (30), and resembling that of tetrapods, with expression boundaries spanning the AP axis of the embryo (4). Furthermore, we have found close qualitative associations between *hox* expression boundaries and anatomical transitions in the skate axial skeleton, with anterior expression limits of *hox* paralogy groups that pattern axial regions in tetrapods also predicting regional transitions in the skate vertebral column. In tetrapods, *hox6*, *-9*, *-10*, and *-11* paralogs pattern the cervical–thoracic, thoracic–lumbar, lumber–sacral, and sacral–caudal transitions, respectively. In the skate, the anterior expression limit of *hox6* group genes corresponds to the position in the synarcual from which the lateral stay projects to articulate with the pectoral girdle (corresponding to spinal nerve foramina 13 to 17), while anterior expression limits of *hox9*, *-10*, and *-11* group genes correspond, respectively, to transitions from R1–R2 (the back of the synarcual), R2–R3, and R4–R5 (the trunk–tail boundary) (Fig. 4).

Some regional distinctions within the skate vertebral column (the synarcual/R1, R3, and R5) are apparent based on qualitative morphological characteristics, while others (R2 and R4) are more subtle and are defined solely based on morphometry. Interestingly, the latter two regions both derive from somites that experience temporal shifts in the expression of single *hox* orthologs. While most of the *hox* genes investigated here show relatively static anterior expression boundaries across developmental stages, anterior limits of *hoxb10* and *hoxa11* expression exhibit conspicuous caudal and rostral shifts, respectively, from embryonic S18 to S25. Somites that experience the caudal shift in *hoxb10* expression contribute to R2, while somites that experience the rostral shift in *hoxa11* expression contribute to R4. Previous work in *Drosophila* has revealed several potential mechanisms in which subtle changes in expression of a single *Hox* gene can affect the patterning of multiple body segments. For example, near-constant expression of UBX protein is required to pattern parasegment 6 in *Drosophila* but, to arrive at the unique set of traits that make up parasegment 5, UBX expression must shift both in position and timing (40). Additionally, recent work in *Drosophila* has highlighted how small dosage-dependent effects of *Atnp* and *Ubx* transcription can impact specification of appendage identity and morphology (41). We suggest that temporal shifts in *hox* transcription in skate could likewise lead to varying doses of hox protein within somites, and could reflect important roles for both qualitative and quantitative *hox* expression features in the establishment of vertebral regions exhibiting greater or lesser degrees of morphological disparity.

Hox genes impart positional identity onto serially homologous structures like body segments and vertebrae in animal groups as diverse as arthropods, annelids, and vertebrates (4, 42–47). This regionalization of segments, in turn, allows for functional specializations that have facilitated morphological change across the evolutionary tree of animals. The striking conservation of *Hox* expression with anatomical boundaries between tetrapods and skate indicates that an elaborate program of *Hox*-based vertebral regionalization did not arise along the tetrapod stem but rather has a much deeper origin, occurring within at least the last common ancestor of jawed vertebrates. Whether this conservation reflects homology of axial skeletal regions between skate and tetrapods or parallel, independent evolution of regionalization from a deeply shared AP program of nested *Hox* expression remains to be seen. Wider taxon sampling and the application of comparative morphometric approaches to identify axial regions across vertebrates has the potential to reveal the complex evolutionary history of this key feature of the vertebrate body plan.

Materials and Methods

Animal Collection and Husbandry. We acquired little skate (*L. erinacea*) adults and embryos from captive brood stock at the Marine Resources Center of the Marine Biological Laboratory (MBL). All animal work complied with protocols approved by the MBL (Institutional Animal Care and Use Committee Protocol No. 19-34). We killed adults and embryos for CT scanning and gene expression analyses, respectively, with an overdose of MS-222 (1 g/L) in seawater, fixed them in 4% paraformaldehyde (1 wk for adults, overnight for embryos), and rinsed them in 1× phosphate-buffered saline (PBS). We then dehydrated adults into 70% ethanol and stored them at room temperature prior to CT scanning, and dehydrated embryos into 100% methanol and stored them at −20 °C prior to gene expression analysis. Skate embryo staging follows Ballard et al. (48) and Maxwell et al. (49).

Skate Vertebral Morphometrics. We scanned three adult little skates at the Cambridge Biotomography Centre using a Nikon XTEK H 225 ST microCT scanner (see *SI Appendix*, Table S4 for scan parameters). We then segmented individual vertebrae up to number 70 (spanning expression boundaries of all potential *hox* genes investigated) from each scan in Mimics v23 (Materialise) or VGSTUDIO MAX v3.2.5 with the Coordinate Measurement module (Volume Graphics) and exported vertebral models as STL files. To collect 3D geometric morphometric data, we plotted a series of 12 homologous landmarks represented by 3D Cartesian grid coordinates on each vertebra using Checkpoint (Stratovan) (Fig. 1 and *SI Appendix*, Table S1). We exported landmarks plotted in Checkpoint as NTS files and combined them into a single file encompassing landmark coordinates for each vertebra in succession. We then imported NTS files into the geomorph R package (50, 51), aligned the coordinates using Procrustes superimposition to account for differences in size and position, and performed a PC analysis (Fig. 1 and *SI Appendix*, Fig. S1 *A*–*C*).

Segmented Linear Regressions and Model Fitting. We tested for vertebral regionalization using a maximum-likelihood and segmented linear regression approach using the regions R package, as described in Jones et al. (3), modified from Head and Polly (38). This method fits iterative regression lines on the slopes of the PC scores from the morphometric analysis, for each potential region model (i.e., two regions, three regions, four regions, etc.), and then the most likely model is selected using the Akaike information criterion, which minimizes the overall residual sum of squares and penalizes against increasing numbers of regions (3, 38). We included the first five PCs in the regionalization score calculation (as in ref. 38).

These analyses tested for region boundaries that potentially align with known tetrapod regions, in the context of *hox* gene expression in skate. To compare region numbers in skate with *Hox*-associated boundaries in the tetrapod precaudal axial skeleton, we selected a four-region maximum (five including the synarcual as the first region) for regression analysis (as in ref. 38). Increasing models to six regions overfit the data and caused the recovery of small and variable region boundaries, whereas a four-region maximum resulted in highly consistent boundaries between the three skate specimens (*SI Appendix*, Figs. S1 *A′*–*C′* and *D* and S5).

Multiple factors affect shape and shape change within the vertebral column. To separate scaling-independent shape variation more likely to result from *hox* expression from allometric shape variation that could be attributable to a process such as intracolumnar differences in growth rate, we regressed PC scores against centroid size for each vertebra using multivariate least-squares regression. Component score residuals from the regression represent the proportion of shape change that is not attributable to allometric scaling, and we performed regionalization analyses on these variables, resulting in nearly identical results to the full shape variable datasets (*SI Appendix*, Fig. S1 *A″*–*C″* and *E*).

Gene Cloning, mRNA In Situ Hybridization, and Vibratome Sectioning. We performed gene cloning and whole-mount mRNA ISH as described in Hirschberger et al. (52) for selected genes within the *hox5* to *11* paralogy groups at S18, S20, S22, and S25, covering the onset to termination of somitogenesis. To precisely determine expression boundaries in selected embryos in which precise anterior expression limits were difficult to count in whole mount (i.e., *hoxa11*), we embedded post-ISH embryos in 15% (weight/volume) gelatin (as described in ref. 35) and sectioned them in sagittal plane using a Leica VT1000S vibratome at 40-μm thickness. We then DAPI-stained and coverslipped tissue sections using Fluoromount-G (Southern Biotech), and imaged slides on a Zeiss Axioscope.

Fate-Mapping Experiments. We cultured skate embryos in their egg cases in flow-through seawater at 10 to 12 °C for approximately 4 wk prior to experimentation at S24. We performed CM-DiI (ThermoFisher) injections in skate embryos as previously described (34), with injections targeting somites at the anterior limits of *hox* gene expression, as determined by our mRNA ISH experiments. After experimentation, we returned the embryos to their egg cases and to seawater tables and cultured them at ∼15 °C until S32. We then killed the embryos with an overdose of ms-222 (tricaine; 1 g/L) and fixed them in 4% paraformaldehyde overnight at 4 °C. After fixation, we washed the embryos 3 × 5 min in 1× PBS, embedded them in 15% gelatin according to Criswell and Gillis (35), and vibratome-sectioned them at 100-μm thickness as discussed above. We imaged tissue sections on an Olympus FV3000 confocal microscope using a 10× objective.

Data Availability. Image stacks representing CT scans of three adult little skates, NTS files including coordinate data from morphometrics landmarks, and an R script with code for regionalization analyses reported in this paper have been deposited in the Environmental Information Data Centre (https://doi.org/10.5285/9d7810c7-92af-47b2-81ec-365aafc39691), managed by the Natural Environment Research Council (53).

hox gene sequences from the little skate for the 14 genes reported in this paper have been deposited in GenBank (accession nos. *hoxa5*, MZ712109; *hoxa6*, OK360934; *hoxa7*, OK360935; *hoxa9*, OK360946; *hoxa10*, OK360936; *hoxa11*, OK360937; *hoxb5*, OK360938; *hoxb6*, OK360939; *hoxb7*, OK360940; *hoxb8*, OK360941; *hoxb10*, OK360942; *hoxd8*, OK360943; *hoxd10*, OK360944; and *hoxd11*, OK360945).

All other study data are included in the article and/or *SI Appendix*.

ACKNOWLEDGMENTS. We thank the members of the J.A.G. and J.J.H. labs for valuable discussions, and Michael Akam for his comments on the manuscript. Keturah Smithson performed microCT scanning of adult skates at the Cambridge Biotomography Centre. We are grateful to the staff of the Marine Resources Center at the Marine Biological Laboratory for assistance in animal husbandry; Dr. Richard Schneider, Prof. David Sherwood, and the MBL Embryology Course for provision of laboratory space; and Louise Bertrand and Leica Microsystems for microscopy support. This project benefited from use of the Imaging Facility, Department of Zoology, supported by a Sir Isaac Newton Trust Research Grant [Reference No. 18.07ii(c)]. This research was funded by a Natural Environment Research Council Grant (to J.J.H., J.A.G., and K.E.C.: NE/S000739/1) and a Royal Society University Research Fellowship (UF130182 and URF\R\191007), Royal Society Research Grant (RG140377), and University of Cambridge Sir Isaac Newton Trust Grant (14.23z) (to J.A.G.).

1. P. E. Ahlberg, J. A. Clack, H. Blom, The axial skeleton of the Devonian tetrapod *Ichthyostega*. *Nature* **437**, 137–140 (2005).
2. J. Müller *et al.*, Homeotic effects, somitogenesis and the evolution of vertebral numbers in recent and fossil amniotes. *Proc. Natl. Acad. Sci. U.S.A.* **107**, 2118–2123 (2010).
3. K. E. Jones *et al.*, Fossils reveal the complex evolutionary history of the mammalian regionalized spine. *Science* **361**, 1249–1252 (2018).
4. A. C. Burke, C. E. Nelson, B. A. Morgan, C. Tabin, *Hox* genes and the evolution of vertebrate axial morphology. *Development* **121**, 333–346 (1995).
5. D. M. Wellik, M. R. Capecchi, *Hox10* and *Hox11* genes are required to globally pattern the mammalian skeleton. *Science* **301**, 363–367 (2003).
6. D. M. Wellik, *Hox* patterning of the vertebrate axial skeleton. *Dev. Dyn.* **236**, 2454–2463 (2007).

7. D. C. McIntyre *et al.*, Hox patterning of the vertebrate rib cage. *Development* **134**, 2981–2989 (2007).
8. M. Mallo, D. M. Wellik, J. Deschamps, Hox genes and regional patterning of the vertebrate body plan. *Dev. Biol.* **344**, 7–15 (2010).
9. M. J. Cohn, C. Tickle, Developmental basis of limblessness and axial patterning in snakes. *Nature* **399**, 474–479 (1999).
10. Y. K. Ohya, S. Kuraku, S. Kuratani, *hox* code in embryos of Chinese soft-shelled turtle *Pelodiscus sinensis* correlates with the evolutionary innovation in the turtle. *J. Exp. Zoolog. B Mol. Dev. Evol.* **304B**, 107–118 (2005).
11. J. M. Woltering *et al.*, Axial patterning in snakes and caecilians: Evidence for an alternative interpretation of the *Hox* code. *Dev. Biol.* **332**, 82–89 (2009).
12. N. Di-Poï *et al.*, Changes in *Hox* genes' structure and function during the evolution of the squamate body plan. *Nature* **464**, 99–103 (2010).
13. J. H. Mansfield, A. Abzhanov, Hox expression in the American alligator and evolution of archosaurian axial patterning. *J. Exp. Zoolog. B Mol. Dev. Evol.* **314**, 629–644 (2010).
14. C. Böhmer, O. W. M. Rauhut, G. Wörheide, New insights into the vertebral Hox code of archosaurs. *Evol. Dev.* **17**, 258–269 (2015).
15. L. Grande, W. E. Bemis, A comprehensive phylogenetic study of amiid fishes (Amiidae) based on comparative skeletal anatomy. An empirical search for interconnected patterns of natural history. *J. Vertebr. Paleontol.* **18** (suppl. 1), 1–696 (1998).
16. K. V. Kardong, *Comparative Anatomy, Function, Evolution* (McGraw-Hill, ed. 5, 2009).
17. A. B. Ward, E. L. Brainerd, Evolution of axial patterning in elongate fishes. *Biol. J. Linn. Soc. Lond.* **90**, 97–116 (2007).
18. N. C. Bird, P. M. Mabee, Developmental morphology of the axial skeleton of the zebrafish, *Danio rerio* (Ostariophysi: Cyprinidae). *Dev. Dyn.* **228**, 337–357 (2003).
19. A. De Clercq *et al.*, Vertebral column regionalisation in Chinook salmon, *Oncorhynchus tshawytscha*. *J. Anat.* **231**, 500–514 (2017).
20. L. A. Jawad, L. Al-Hassani, Morphological study of the ponyfish *Leiognathus equulus* (family: Leiognathidae) collected from the Sea of Oman. *Int. J. Mater. Sci.* **4**, 10.5376/ijms.2014.04.0033 (2014).
21. L. C. Sallan, Tetrapod-like axial regionalization in an early ray-finned fish. *Proc. Biol. Sci.* **279**, 3264–3271 (2012).
22. V. E. Prince, L. Joly, M. Ekker, R. K. Ho, Zebrafish *hox* genes: Genomic organization and modified colinear expression patterns in the trunk. *Development* **125**, 407–420 (1998).
23. D. G. Ahn, G. Gibson, Expression patterns of threespine stickleback hox genes and insights into the evolution of the vertebrate body axis. *Dev. Genes Evol.* **209**, 482–494 (1999).
24. A. G. Hayward, II, P. Joshi, I. Skromne, Spatiotemporal analysis of zebrafish *hox* gene regulation by Cdx4. *Dev. Dyn.* **244**, 1564–1573 (2015).
25. E. M. Morin-Kensicki, E. Melancon, J. S. Eisen, Segmental relationship between somites and vertebral column in zebrafish. *Development* **129**, 3851–3860 (2002).
26. P. Sordino, D. Duboule, T. Kondo, Zebrafish Hoxa and Evx-2 genes: Cloning, developmental expression and implications for the functional evolution of posterior Hox genes. *Mech. Dev.* **59**, 165–175 (1996).
27. F. van der Hoeven, P. Sordino, N. Fraudeau, J.-C. Izpisúa-Belmonte, D. Duboule, Teleost HoxD and HoxA genes: Comparison with tetrapods and functional evolution of the HOXD complex. *Mech. Dev.* **54**, 9–21 (1996).
28. Z. Ye, D. Kimelman, Hox13 genes are required for mesoderm formation and axis elongation during early zebrafish development. *Development* **147**, dev185298 (2020).
29. K. D. Economides, L. Zeltser, M. R. Capecchi, *Hoxb13* mutations cause overgrowth of caudal spinal cord and tail vertebrae. *Dev. Biol.* **256**, 317–330 (2003).
30. S. Oulion *et al.*, Evolution of repeated structures along the body axis of jawed vertebrates, insights from the *Scyliorhinus canicula* Hox code. *Evol. Dev.* **13**, 247–259 (2011).
31. R. Freitas, G. Zhang, M. J. Cohn, Biphasic Hoxd gene expression in shark paired fins reveals an ancient origin of the distal limb domain. *PLoS One* **2**, e754 (2007).
32. F. Berio, Y. Bayle, C. Riley, O. Larouche, R. Cloutier, Phenotypic regionalization of the vertebral column in the thorny skate *Amblyraja radiata*: Stability and variation. *J. Anat.*, 10.1111/joa.13551 (2021).
33. K. E. Criswell, M. I. Coates, J. A. Gillis, Embryonic development of the axial column in the little skate, *Leucoraja erinacea*. *J. Morphol.* **278**, 300–320 (2017).
34. K. E. Criswell, M. I. Coates, J. A. Gillis, Embryonic origin of the gnathostome vertebral skeleton. *Proc. Biol. Sci.* **284**, 20172121 (2017).
35. K. E. Criswell, J. A. Gillis, Resegmentation is an ancestral feature of the gnathostome vertebral skeleton. *eLife* **9**, e51696 (2020).
36. Z. Johanson, K. Martin, G. Fraser, K. James, The synarcual of the little skate, *Leucoraja erinacea*: Novel development among the vertebrates. *Front. Ecol. Evol.* **7**, 10.3389/fevo.2019.00012 (2019).
37. K. M. Claeson, The synarcual cartilage of batoids with emphasis on the synarcual of Rajidae. *J. Morphol.* **272**, 1444–1463 (2011).
38. J. J. Head, P. D. Polly, Evolution of the snake body form reveals homoplasy in amniote *Hox* gene function. *Nature* **520**, 86–89 (2015).
39. B. L. King, J. A. Gillis, H. R. Carlisle, R. D. Dahn, A natural deletion of the *HoxC* cluster in elasmobranch fishes. *Science* **334**, 1517 (2011).
40. J. Castelli-Gair, M. Akam, How the Hox gene Ultrabithorax specifies two different segments: The significance of spatial and temporal regulation within metameres. *Development* **121**, 2973–2982 (1995).
41. R. Paul *et al.*, Hox dosage contributes to flight appendage morphology in *Drosophila*. *Nat. Commun.* **12**, 2892 (2021).
42. M. Akam, Hox genes and the evolution of diverse body plans. *Philos. Trans. R. Soc. Lond. B Biol. Sci.* **349**, 313–319 (1995).
43. M. Averof, N. H. Patel, Crustacean appendage evolution associated with changes in Hox gene expression. *Nature* **388**, 682–686 (1997).
44. C. L. Hughes, T. C. Kaufman, Hox genes and the evolution of the arthropod body plan. *Evol. Dev.* **4**, 459–499 (2002).
45. M. Kulakova *et al.*, Hox gene expression in larval development of the polychaetes *Nereis virens* and *Platynereis dumerilii* (Annelida, Lophotrochozoa). *Dev. Genes Evol.* **217**, 39–54 (2007).
46. P. R. H. Steinmetz, R. P. Kostyuchenko, A. Fischer, D. Arendt, The segmental pattern of *otx*, *gbx*, and Hox genes in the annelid *Platynereis dumeriliі*. *Evol. Dev.* **13**, 72–79 (2011).
47. J. M. Serano *et al.*, Comprehensive analysis of Hox gene expression in the amphipod crustacean *Parhyale hawaiensis*. *Dev. Biol.* **409**, 297–309 (2016).
48. W. W. Ballard, J. Mellinger, H. Lechenault, A series of normal stages for development of *Scyliorhinus canicular*, the lesser spotted dogfish (*Chondrichthyes: Scyliorhinidae*). *J. Exp. Zool.* **267**, 318–336 (1993).
49. E. E. Maxwell, N. B. Fröbisch, A. C. Heppleston, Variability and conservation in late chondrichthyan development: Ontogeny of the winter skate (*Leucoraja ocellata*). *Anat. Rec. (Hoboken)* **291**, 1079–1087 (2008).
50. E. Baken, M. Collyer, A. Kaliontzopoulou, D. Adams, geomorph v4.0 and gmShiny: Enhanced analytics and a new graphical interface for a comprehensive morphometric experience. *Methods Ecol. Evol.*, 10.1111/2041-210X.13723 (2021).
51. D. Adams, M. Collyer, A. Kaliontzopoulou, E. Baken, Geomorph: Software for Geometric Morphometric Analyses (R Package Version 3.1.2, 2019). https://cran.r-project.org/web/packages/geomorph/index.html. Accessed 30 September 2019.
52. C. Hirschberger, V. A. Sleight, K. E. Criswell, S. J. Clark, J. A. Gillis, Conserved and unique transcriptional features of pharyngeal arches in the skate (*Leucoraja erinacea*) and evolution of the jaw. *Mol. Biol. Evol.* **38**, 4187–4204 (2021).
53. K. E. Criswell, J. J. Head, J. A. Gillis, Morphological and morphometric data on the axial skeleton of the little skate, *Leucoraja erinacea*. NERC EDS Environmental Information Data Centre. https://www.ncbi.nlm.nih.gov/nuccore/?term=OK360937. Deposited 29 November 2021.